Design of a New Bio-Inspired Dual-Axis Compliant Micromanipulator with Millimeter Strokes

Zekui Lyu and Qingsong Xu, *Senior Member, IEEE*

***Abstract*— This paper proposes the concept design of a novel bio-inspired dual-axis compliant micromanipulator with millimeter working strokes dedicated to fiber alignment. It subtly mimics the gripping and rubbing function of the human hand consisting of the forefinger, purlicue, and thumb. Compared with traditional dual-axis grippers, its advantages lie in millimeter-level stroke, bi-directional rotation, less slippage, and comprehensive force sensing. To achieve dexterous and reliable manipulation, a two-degree-of-freedom (2-DOF) flexible decoupling mechanism and a displacement reversing mechanism based on the leaf-shaped flexible hinge are introduced. A prototype driven by two voice coil motors is fabricated for experimental testing. Three high-precision strain gauges with temperature compensation are glued on the sensitive region to measure the gripping force and rubbing force. Experimental results show that the gripping and rubbing strokes of the manipulator are up to 2.3 mm and 2.1 mm, respectively. For a custom-made fiber flag with a diameter of 200 μm, the rotation stroke of more than 1000° has been achieved, which cannot be realized by previous work with the same level of compact mechanism design.**

I. Introduction

The manipulator with gripping and rubbing functions has promising applications in precision operations such as fiber alignment [1]–[3]. For example, inspired by the usage of chopsticks to grip, rub, and release food, Wang et al. proposed a dual-axis asymmetric micromanipulator driven by piezoelectric actuators (PZT) and demonstrated the precise gripping and rubbing of fine wire and flag [4]. Similarly, some other compliant dual-axis manipulators have been designed for 2-DOF manipulation in fiber alignment [5]–[8]. Xu introduced a compliant modular microgripper with 2-DOF parallel translational motion based on four PZTs to reduce the maintenance cost [5]. However, the relatively low amplification ratio (2.43 and 2.48) is a shortcoming. Afterward, the improvement of the magnification ratio and the detection of operating force became the key issue for the design of the 2-DOF manipulator. Chen et al. developed a 2-DOF microgripper by utilizing two lever mechanisms as displacement amplifiers, which produced 190 μm stroke in the left tip and 85 μm stroke in the right tip [1]. The grasping force was measured via a strain gauge glued on double flexural beams of the left gripping jaw. Dsouza et al. presented an analogous compliant microgripper using the large amplification ratio of the series lever mechanism, and the gripping force was measured by the non-contact visual servo method [6]. To avoid the impact of non-parallel operation during fiber manipulation, two flexible parallelogram mechanisms were adopted by Zhang et al. to linearize the output of the manipulator [7]. However, these manipulators only considered the monitoring of the gripping force during manipulation. In some other work, the gripping force on one side and the rubbing force on the other side were measured simultaneously [4], [8]. Whereas in the process of rotating the fiber, the monitoring of the reaction force of the fiber on the gripping side mechanism is indirect. Additionally, if the end of the manipulator is not provided with a V-shaped groove to hold the fiber, longitudinal slip is inevitable in the process of rotating [4], which will reduce the working stroke. Actually, high-precision manufacturing of the V-groove and accurate placement of the fiber is a complicated and time-consuming process. Therefore, the currently available 2-DOF manipulator still needs to be improved in terms of operation manner, working stroke, and so on.

It is well-known that the sophisticated structure and complex functions of the human hand are incomparable to many manipulators. In the literature, a large number of manipulator designs have been derived based on a simplified structure [9]–[11]. Herein, we pay attention to the gripper-like component consisting of the forefinger, purlicue, and thumb (GCFPT), as shown in Fig. 1(a). GCFPT can realize the actions such as gipping, rubbing, pinching, ejecting, etc., by manipulating the forefinger and thumb. Furthermore, the two actions of gripping and rubbing are expected functions of the manipulator for use in fiber alignment. These two functions of GCFPT are decomposed as shown in Fig. 1(b) and (c). The forefinger and thumb are replaced with two gripping arms, respectively, to complete the demonstration of the manipulation function. When gripping a target, the thumb usually remains relatively stationary while the forefinger moves downward to form a close. When rubbing the target, the forefinger and thumb offer opposite motion trends, such as forward movement of the forefinger and backward motion of the thumb. Obviously, it is different from the motion scheme of the previously designed 2-DOF gripper. In the grippers reported in the literature, only one side of the gripper moves while the other side remains static during the rubbing manipulation. Fig. 1(d) demonstrates that the object slides forward while rotating when only one side force (F_{r1}) is applied. This is because shifting the thrust towards the objects center of mass (virtual $F_{r1}^{'}$ and its balance force

This work was supported in part by the National Natural Science Foundation of China under Grant 52175556, the Macao Science and Technology Development Fund under Grant 0022/2019/AKP, 0153/2019/A3 and 0102/2022/A2, and Research Committee of the University of Macau under Grant MYRG2022-00068-FST and MYRG-CRG2022-00004-FST.

The authors are with the Department of Electromechanical Engineering, Faculty of Science and Technology, University of Macau, Macau, China.

Corresponding author: Q. Xu (phone: +853-88224278; fax: +853-88222426; e-mail: qsxu@umac.mo).

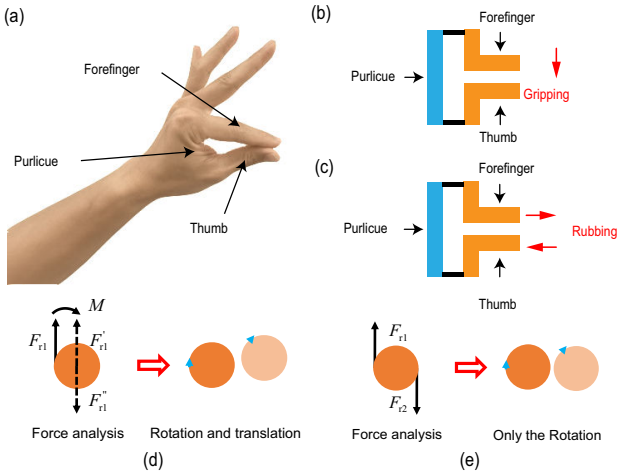

Fig. 1. Illustration of the forefinger, purlicue, and thumb (GCFPT). (a) GCFPT, (b) gripping operation mode, (c) rubbing operation mode, (d) previous manipulating manner, and (e) novel manipulating manner.

F''_{r1}) causes a little moment (M), which is known from theoretical mechanics. This situation does not occur in Fig. 1(e), however, since they are driven in different ways. When the two sides of a tiny target are subjected to two forces (F_{r1} and F_{r2}) of equal value but in opposite directions, it will rotate due to the action of the moment without slipping. Therefore, the object rotated steadily when it was handed by the GCFPT.

In this paper, a new GCFPT-inspired 2-DOF manipulator is designed and developed to reinforce the manipulation capability. The compliant mechanism is selected to construct the gripping and rubbing function of the GCFPT to be imitated owing to its excellent performance [12]–[14]. There are still three issues that need to be considered and addressed in manipulator design. The first one is the type selection and quantity restriction of actuators. Voice coil motors (VCM) have been adopted due to the characteristics of large output stroke, good force characteristics, and convenient control [15], [16]. In addition, to avoid complicated mechanical mechanisms and troublesome control systems, the number of actuators is limited to two. Second, the grasping arm that imitates the forefinger needs to be able to grip and rub simultaneously with 2-DOF motion. It means that the mechanism of the manipulator on this side needs to be totally decoupled at the input and output ends. Third, when performing the rubbing operation, a single actuator is expected to make the two gripping arms move in reverse synchronization. In other words, the gripping arm that mimics the thumb needs to perform an equal-rigidity reverse movement relative to the forefinger arm. These requirements impose severe challenges to the architecture design of the GCFPT-inspired manipulator.

To this end, this paper presents the design and experimental testing of a novel 2-DOF compliant manipulator inspired by GCFPD. The dimension, workspace, and area ratio of some typical 2-DOF manipulators are tabulated in Table I. The index of area ratio (η) is defined to assess

TABLE I
AREA RATIO OF TYPICAL 2-DOF MANIPULATORS

Reference	Dimension (mm^2)	Workspace (mm^2)	Area ratio (%)
[1]	58×34	0.19×0.085	0.00082
[2]	67.45×49	0.251×0.225	0.00171
[4]	68×58	0.223×0.093	0.00053
[6]	55×50	0.241×0.134	0.00117
[7]	50×35	0.164×0.083	0.00078
[8]	62×50	0.108×0.224	0.00078
This work	200×150	2.3×2.1	0.01610

the compactness of the mechanism, and its expression is given as $\eta = \frac{S_g \times S_r}{L \times W}$. S_g and S_r represent the gripping stroke and rubbing stroke of the manipulator (in a unit of a millimeter), while L and W denote the length and width of the structure (in a unit of a millimeter), respectively. The larger the ratio, the more compact the mechanism. Many researchers have recognized this metric as an index to assess the area usage efficiency of a micro-positioning platform or microgripper in previous studies [17], [18]. It is evident that the designed 2-DOF manipulator provides the highest area ratio, which has the potential to be scaled down to a small size with a corresponding workspace. In addition, the millimeter-level working stroke, two rotating directions, less slippage, and comprehensive force-sensing guarantee the efficiency and reliability of fiber manipulation. These advantages benefit from the large-stroke actuation of the VCM and elastic displacement transmission of the leaf-shaped flexible hinges. The 2-DOF decoupling flexible platform and the displacement reversing mechanism based on the leaf-shaped flexible hinges are dominant components of the manipulator. The concept design and experimental validation of the proposed manipulator are carried out in the following sections to examine its performance.

II. CONCEPT DESIGN AND MECHANICAL FABRICATION

The overall mechanism of the proposed 2-DOF compliant manipulator inspired by GCFPD is designed as shown in Fig. 2. It mainly consists of two VCMs and their fixing base, two connectors, a manipulator, a base, fixed screws, and other parts. A 2-DOF decoupling flexible platform (DFP) is designed for the manipulator's left side, while a modified compliant displacement reversing mechanism (DRM) is adopted in the right arm. Two VCM actuators are arranged orthogonally on either side of the gripper. In particular, VCM-1 drives the mechanism to perform the parallel gripping operation, and VCM-2 provides the actuation for the rubbing action. The two VCMs are connected to the gripper via connector-1 and 2 for transferring the force and displacement. Double compound fixed-guide beam mechanism (DCFBM) 1–3 facilitates the transmission of the actuation motion and also isolates the interference of the displacement in other directions to the actuators. Furthermore, DCFBM 4 and the basic compliant parallelogram mechanism (BCMP) 5 realize the transmission and decoupling of the output displacement of the left gripper in two directions. DCFBM 6 and compound fixed-guide beam

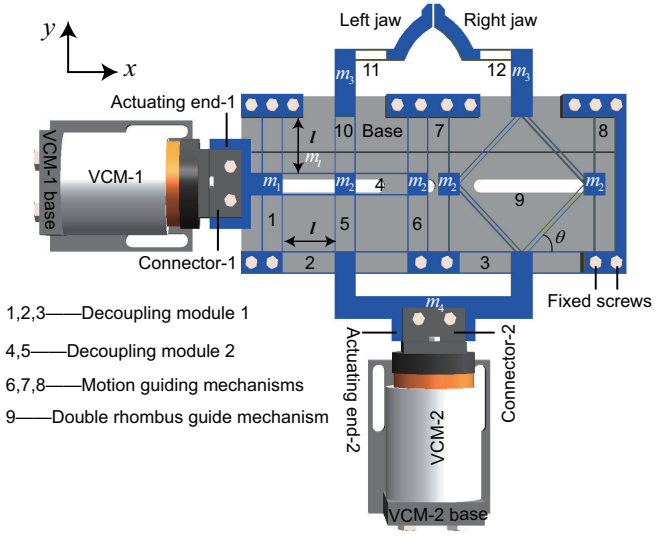

Fig. 2. CAD model of the designed 2-DOF compliant manipulator inspired by GCFPD.

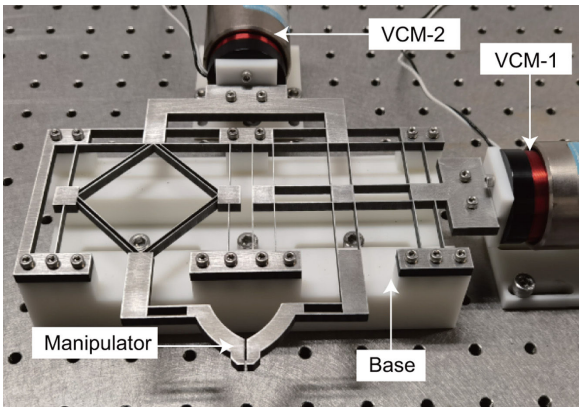

Fig. 3. Photograph of the developed 2-DOF manipulator: the assembled prototype.

mechanism (CFBM) 7–8 play an indispensable role in the displacement guide. The double-layer compliant rhombus-shaped mechanism 9 (DCRM) is adopted for displacement transmission and direction change because its longitudinal stiffness is much greater than the lateral stiffness. The left and right jaws with double flexural beams are connected to the two sides of the mechanism and extend slightly from the base to facilitate the manipulation of relatively small targets.

When VCM-1 receives a positive driving current, the left jaw moves to the right in parallel to grip the target in the gap, which is a normally open gripper. In contrast, when VCM-1 is subjected to a reversing current input, the left jaw is pulled to the left. After the large target enters the gap, the flexure hinge can recover the deformation and grasp the object. This is a normally closed gripping method. When the coil of VCM-2 moves upward, the left jaw also moves upward and the right jaw shifts downward to perform a clockwise rubbing of the target, and vice versa. If a positive or negative current is applied to the VCM-2, the rotation directions of the two operating jaws are different. So, the rotating direction of the

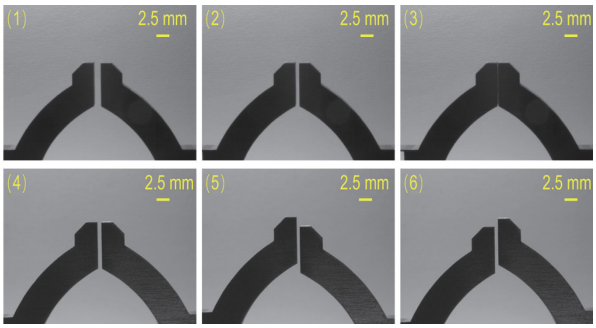

Fig. 4. The movement of the manipulator's jaws.

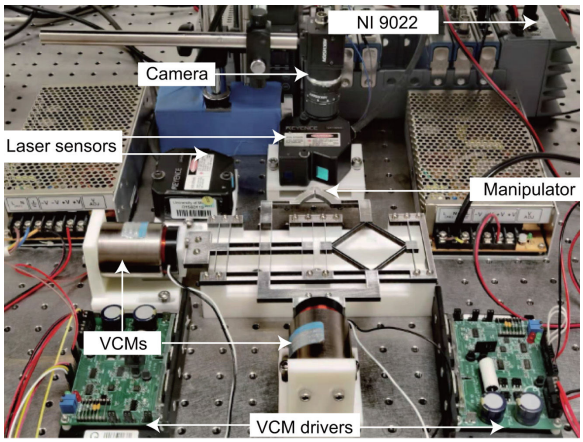

Fig. 5. Photograph of the experimental testing system.

fiber could be in a clockwise or counterclockwise direction.

Through several optimization iterations, the main structural parameters of the manipulator are determined. The overall size of the manipulator is about 200 mm × 150 mm × 5 mm without VCMs, and the compact architecture is conducive to its application in practice. For a more detailed model analysis and numerical simulation of the designed manipulator please refer to the journal version of this paper [19]. The manipulator is manufactured from a piece of Al-7075 alloy plate by the wire electrical discharge machining technology. The Al-7075 alloy exhibits good mechanical properties and is commonly used in the manufacture of flexible mechanisms. The assembled manipulator is immobilized on a vibration isolation platform, as shown in Fig. 3. In addition, Fig. 4 exhibits the position of the gripping/rubbing jaw of the manipulator in different working conditions. Taking state (2) as the initial state, states (1) and (3) show the expansion and contraction of the jaw gap, respectively. Similarly, considering state (4) as a benchmark, states (5) and (6) display the different positions of the jaws moving forward and backward, respectively. These results qualitatively demonstrate that the manufactured manipulator has gripping and rubbing capabilities. To make a quantitative evaluation, more experiments are conducted in the following, and Fig. 5 shows the experimental setup.

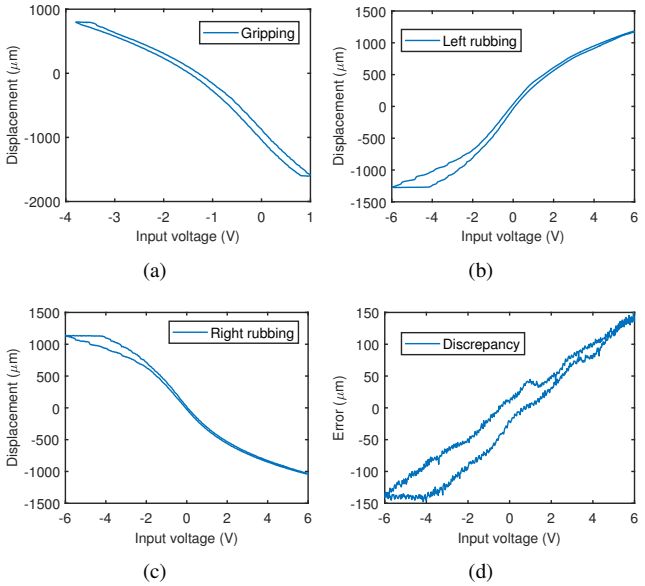

Fig. 6. Experiment results of working stroke. (a) Gripping stroke, (b) left rubbing stroke, (c) right rubbing stroke, and (d) discrepancy between two sides of rubbing mechanism.

III. Experimental Validation and Performance Comparison

The working stroke of the manipulator is an important index. Here, the gripping stroke, left rubbing stroke, and right rubbing stroke of the manipulator are obtained as $[-1604.31, 791.08]$ μm, $[-1266.86, 1183.26]$ μm, and $[-1039.11, 1137.50]$ μm, respectively, as shown in Fig. 6. Meanwhile, the hysteresis phenomenon of the manipulator in the working process has been observed, which is caused by the hysteresis of VCM output (with an input frequency of 0.5 Hz). When the manipulator is rubbing, the left and right sides of the machine move forward and backward simultaneously, and the stroke error is shown in Fig. 6(d). There are three reasons for this error. First, the equal stiffness of both sides is deduced on the basis of the assumption of small deformation and ignoring the compression energy loss of part of LSFH, which induces a theoretical error. Second, there are inevitable errors on both sides of the manufacturing process. Third, the uneven force on both sides of the mechanism is the main cause of the experimental error. In this work, the VCM is arranged on the central axis of the rubbing mechanism. Due to the presence of assembly error, the output force may deviate from the central axis. As a result, the forces on both sides of the rubbing mechanism are inconsistent. Moreover, it is observed that the natural frequencies in the gripping and rubbing directions of the manipulator are 112.5 Hz and 175.1 Hz, respectively. This indicates that the manipulator has good dynamic characteristics to perform the high-speed operations.

The position resolution is another critical performance of the motion mechanism for both sides of the manipulator. The resolution was obtained with the help of a proportional-integral (PI) controller. A series of stairway-type signals

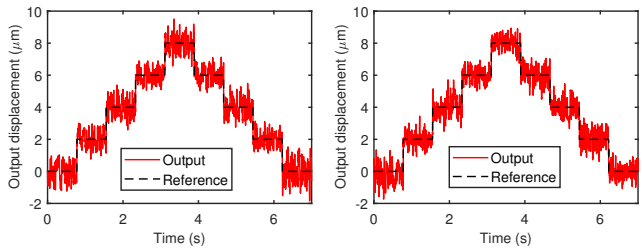

Fig. 7. Experiment results of resolution testing. (a) Gripping motion, and (b) left rubbing motion.

with an amplitude of 2 μm have been applied to the input ends, and the output displacements are measured by a laser displacement sensor. Experimental results of displacement resolution for the gripping and rubbing sides are shown in Fig. 7(a) and (b), respectively. The errors between the reference signals and measurement signals follow the normal distribution with a standard deviation σ, and $2\sigma = 1$ μm is obtained with a 95% confidence interval. Hence, the motion resolutions for both sides of the manipulator are derived as ± 1 μm.

For testing the gripping and rubbing performances of the manipulator, three strain gauges are pasted on the double flexural beams 10, 11, and 12 (see Fig. 2). The sensitivity coefficient of the high-precision resistance strain gauges is 2.0. The strain gauges are connected by bridge circuits with temperature compensation. Before use, the strain-gauge sensors are calibrated by hanging standard weights. The output voltages of the strain gauges exhibit a linear relationship with the exerted weights. By least-square fitting, the linear slope (i.e., sensitivity coefficient) is obtained as 3252.5 mN/mV, 5787.4 mN/mV, and 4789 mN/mV with correlation coefficient of 0.9996, 0.9995, and 0.9987, respectively. Moreover, the measurement accuracy of the three strain-gauge force sensors is obtained as 3.90 mN, 5.08 mN, and 4.92 mN, respectively.

The experimental setup for the gripping and rubbing performance testing of the manipulator is shown in Fig. 8(a). For illustration, a small rectangular paper and fiber with a diameter of 200 μm are glued together to form a fiber flag as the manipulation target. Meanwhile, a custom-built clamp is fabricated by using two bolts and a resin base. The fiber flag is grasped by the clamp which is mounted on a vibration isolation table. Initially, the fiber flag passes through the gap between the two jaws of the manipulator. Then, the actuation current of VCM-1 is increased gradually to reduce jaw clearance. Next, the lower clamp is loosened and the small flag is successfully grasped by the manipulator. Finally, a driving current is applied to VCM-2, so that the flag is rubbed and rotated by the two jaws.

The gripping displacement and gripping force are measured by laser displacement sensor and strain-gauge sensor, respectively. The results are shown in Fig. 8(b), which is divided into two areas A and B, corresponding to the two states before and after the contact between the gripper jaw

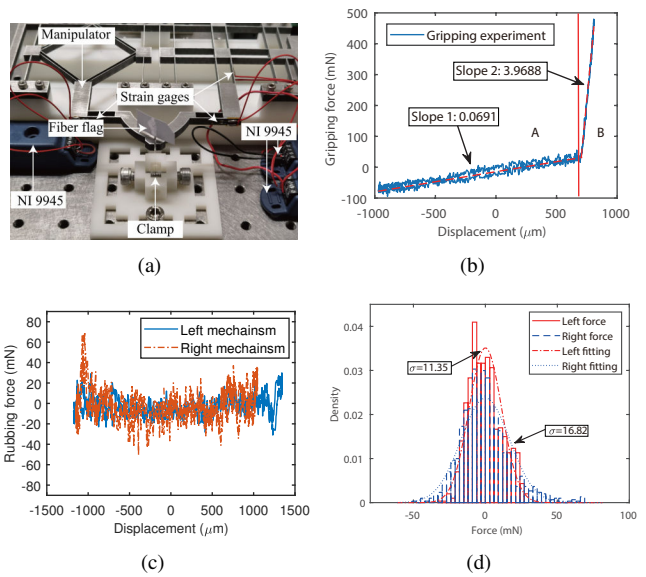

Fig. 8. Experimental testing results of gripping and rubbing. (a) Experimental setup, (b) gripping testing result, (c) rubbing testing result, and (d) noise histogram of rubbing forces on both sides.

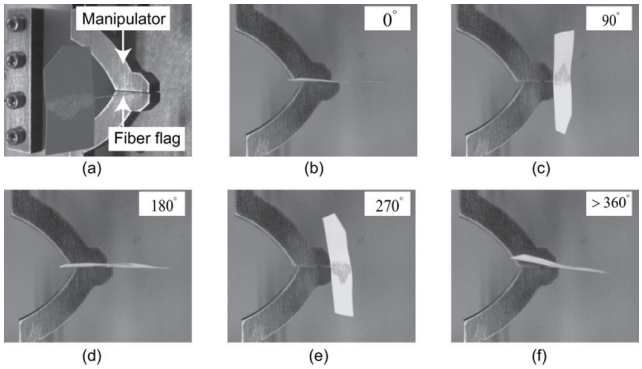

Fig. 9. Snapshots of the gripping and rubbing experiments.

and optical fiber, respectively. Before the left gripper touches the fiber, the strain-gauge sensor output rises slowly and linearly as the increase of actuation displacement. The small slope (S_1) is derived by a linear fitting as 0.0691 mN/μm. This phenomenon is due to the fact that the bottom platform of the double flexural beam moves to the right, the mass of the top mechanism is relatively large, and there is an inertial hysteresis. Hence, the double flexural beams have slight tensile deformation. Once the two parts contact, as the displacement increases slowly, the output force rises rapidly with the slope (S_1) of 3.9688 mN/μm. This indicates that the force output signal caused by the gripping force is much greater than the inertia factor. To obtain an accurate value of the gripping force, the influence of inertia on the mechanism needs to be eliminated. Assuming that the coordinates in the force-displacement image at the time of first contact are (X_1, Y_1), and the coordinates in the final gripping state are (X_2, Y_2). Then, the actual gripping force F_g can be derived and expressed as follows.

$$F_g = (Y_2 - Y_1) - (X_2 - X_1) \cdot S_1. \tag{1}$$

Based on the above equation, the gripping force is calculated as 438.96 mN after eliminating the influence of inertia.

In addition, the displacement and force in the rubbing testing are measured, as depicted in Fig. 8(c). When the manipulator performs the rubbing operation, one side of the strain gauge is compressed, and the other side is pulled. Thus, the signs of the output signals are opposite. It is observed that the fluctuation range of the main force signal (provided by the sensors on both sides) is similar. Normal fitting is made for the rubbing forces on both sides, as shown in Fig. 8(d). The standard deviation of the rubbing force on the two sides is calculated as 11.35 mN and 16.82 mN, respectively. When the rotating mechanism on both sides executes the rubbing operation of the flag, the force discrepancy is about 10.94 mN with a 95% confidence interval. It indicates that the force exerted by the gripping jaws on both sides of the fiber is more balanced when rubbing the fiber, thereby reducing the slippage of the fiber caused by undesirable moments. Previous work in the literature has not conducted such a comparison study on the detection of rubbing force on both sides.

In the gripping and rubbing test experiments, the photos of different motion states of fiber flags are shown in Fig. 9. Fig. 9(b) shows that the flag is successfully held in the air, while the lower clamp is removed. Fig. 9(b)–(f) displays the snapshots of different moments when the small flag is rubbed. The rotation angle over 360° is observed. In fact, the fiber can be manipulated to rotate for about 3 cycles. During the operation, the potential slip of the fiber is negligible. Such a large operation stroke is difficult to be achieved by piezoelectrically actuated dual-axis micromanipulators. Therefore, the designed micromanipulator can greatly improve the efficiency and stability of fiber alignment.

The performances of typical 2-DOF manipulators with gripping and rubbing functions are compared as tabulated in Table II. To facilitate a comprehensive understanding of the 2-DOF manipulator, another two MEMS microgrippers driven by electrothermal actuators (ETA) and electrostatic actuators (ESA) are also considered [20], [21]. The electrothermal or electrostatic actuation microgripper has a very small output stroke and high resolution, which has been presented for the manipulation of particles or single epidermal plant cells. The piezoelectric-actuated 2-DOF microgripper needs to employ a complex multistage displacement amplification mechanism for obtaining the ideal output stroke. However, their working stroke is still difficult to exceed 1 mm. The multi-stage amplifying mechanism will lead to a non-linear increase in output displacement and a decrease in output force. Obviously, compared with these microgrippers, the GCFPD-inspired manipulator proposed in this paper based on VCM has the advantages of millimeter-level output stroke, bi-direction operation, and comprehensive force sensing. These properties will improve the efficiency, flexibility, reliability, and safety during fiber alignment operation. The improvement of motion resolution and further optimization

TABLE II

PERFORMANCE COMPARISON OF 2-DOF COMPLIANT MANIPULATORS DRIVEN BY DIFFERENT ACTUATORS

Ref.	Actuators	Gripping stroke (μm)	Rubbing stroke (μm)	Natural frequency (Hz)	Resolution (μm)	Gripping force sensing	Rubbing force sensing	Gripping direction	Rubbing direction	Dimension (mm^2)	Area ratio (%)
[20]	ETA$\times$4	17	11	-/-	-	-	-/-	1	2	-	-
[21]	ESA$\times$2	16	16	-/-	0.02	Yes	Yes/-	2	2	7×10.8	0.00034
[1]	PZT$\times$2	190	85	221/1003	-	Yes	-/-	1	1	58×34	0.00082
[2]	PZT$\times$2	251	225	350.63/603.37	1.2	Yes	-/-	1	1	67.45×49	0.00171
[4]	PZT$\times$2	222.4	92.8	-/-	0.15	Yes	-/Yes	1	1	68×58	0.00053
[6]	PZT$\times$2	240.53	133.34	-/-	-	Yes	-/-	1	1	55×50	0.00117
[7]	PZT$\times$2	163.3	83.1	326.8/599.5	0.4	Yes	-/-	1	1	50×35	0.00078
[8]	PZT$\times$2	108	223.4	-/-	0.5	Yes	-/Yes	1	1	62×50	0.00078
This work	VCM$\times$2	2395.39	2176.61	112.5/175.1	1	Yes	Yes/Yes	2	2	200×150	0.01610

of the structure will be conducted in future research. Higher-precision laser interferometers and advanced control strategies will be utilized to improve the displacement resolution.

IV. CONCLUSION

The main contribution of the paper lies in the design and development of a dual-axis compliant manipulator inspired by GCFPD to realize the large working stroke and reliable manipulation. Millimeter-level motion and comprehensive force measurement are implemented to increase the efficiency and safety of fiber manipulation. The designed manipulator is composed of an improved 2-DOF flexible decoupling platform and a displacement reversing mechanism. A comparison study indicates that the reported 2-DOF manipulator provides a more compact design with larger strokes than the existing designs. The working strokes of the manipulator are 2.3 mm and 2.1 mm for the gripping motion and rubbing motion, respectively. The measuring accuracy of the gripping force, left rubbing force, and right rubbing force are 3.9 mN, 5.08 mN, and 4.92 mN, respectively. In the rotating test of a fiber flag, the discrepancy of the rubbing force between the two jaws is kept within 10.94 mN, which demonstrates the stability of the operation. During the experiment, the fiber with a diameter of 200 μm was successfully grasped and rotated for about 3 cycles, which cannot be accomplished by the previous designs.

REFERENCES

[1] W. Chen, X. Shi, W. Chen, and J. Zhang, "A two degree of freedom micro-gripper with grasping and rotating functions for optical fibers assembling," *Review of Scientific Instruments*, vol. 84, no. 11, p. 115111, 2013.

[2] Z. Lyu, Q. Xu, and L. Zhu, "Design and development of a new piezoelectric-actuated biaxial compliant microgripper with long strokes," *IEEE Transactions on Automation Science and Engineering*. doi: 10.1109/TASE.2022.3145670, (in press).

[3] Q. Xu, *Design and Implementation of Large-Range Compliant Micropositioning Systems*. John Wiley & Sons, 2016.

[4] F. Wang, B. Shi, Y. Tian, Z. Huo, X. Zhao, and D. Zhang, "Design of a novel dual-axis micromanipulator with an asymmetric compliant structure," *IEEE/ASME Transactions on Mechatronics*, vol. 24, no. 2, pp. 656–665, 2019.

[5] Q. Xu, "Mechanism design and analysis of a novel 2-DOF compliant modular microgripper," in *Proc. of 2012 7th IEEE Conference on Industrial Electronics and Applications (ICIEA)*, pp. 1966–1971, 2012.

[6] R. D. Dsouza, K. P. Navin, T. Theodoridis, and P. Sharma, "Design, fabrication and testing of a 2 DOF compliant flexural microgripper," *Microsystem Technologies*, vol. 24, no. 9, pp. 3867–3883, 2018.

[7] W. Chen, J. Qu, W. Chen, and J. Zhang, "A compliant dual-axis gripper with integrated position and force sensing," *Mechatronics*, vol. 47, pp. 105–115, 2017.

[8] J. Zhang, K. Lu, W. Chen, J. Jiang, and W. Chen, "Monolithically integrated two-axis microgripper for polarization maintaining in optical fiber assembly," *Review of Scientific Instruments*, vol. 86, no. 2, p. 025105, 2015.

[9] L. B. Bridgwater, C. Ihrke, M. A. Diftler, M. E. Abdallah, N. A. Radford, J. Rogers, S. Yayathi, R. S. Askew, and D. M. Linn, "The robonaut 2 hand-designed to do work with tools," in *Proc. of 2012 IEEE International Conference on Robotics and Automation*, pp. 3425–3430, 2012.

[10] Z. Li, Z. Hou, Y. Mao, Y. Shang, and L. Kuta, "The development of a two-finger dexterous bionic hand with three grasping patterns-nwafu hand," *Journal of Bionic Engineering*, vol. 17, no. 4, pp. 718–731, 2020.

[11] S. R. Kashef, S. Amini, and A. Akbarzadeh, "Robotic hand: A review on linkage-driven finger mechanisms of prosthetic hands and evaluation of the performance criteria," *Mechanism and Machine Theory*, vol. 145, p. 103677, 2020.

[12] M. Ling, L. L. Howell, J. Cao, and G. Chen, "Kinetostatic and dynamic modeling of flexure-based compliant mechanisms: a survey," *Applied Mechanics Reviews*, vol. 72, no. 3, p. 030802, 2020.

[13] X. Herpe, R. Walker, M. Dunnigan, and X. Kong, "On a simplified nonlinear analytical model for the characterisation and design optimisation of a compliant XY micro-motion stage," *Robotics and Computer-Integrated Manufacturing*, vol. 49, pp. 66–76, 2018.

[14] A. Al-Jodah, B. Shirinzadeh, M. Ghafarian, T. K. Das, and J. Pinskier, "Design, modeling, and control of a large range 3-DOF micropositioning stage," *Mechanism and Machine Theory*, vol. 156, p. 104159, 2021.

[15] S. Awtar and G. Parmar, "Design of a large range XY nanopositioning system," *Journal of Mechanisms and Robotics*, vol. 5, no. 2, p. 021008, 2013.

[16] Y. Liu and Z. Zhang, "A large range compliant XY nano-manipulator with active parasitic rotation rejection," *Precision Engineering*, vol. 72, pp. 640–652, 2021.

[17] Q. Xu, "New flexure parallel-kinematic micropositioning system with large workspace," *IEEE Transactions on Robotics*, vol. 28, no. 2, pp. 478–491, 2011.

[18] T. K. Das, B. Shirinzadeh, A. Al-Jodah, M. Ghafarian, and J. Pinskier, "Computational parametric analysis and experimental investigations of a compact flexure-based microgripper," *Precision Engineering*, vol. 66, pp. 363–373, 2020.

[19] Z. Lyu and Q. Xu, "Design of a new bio-inspired dual-axis compliant micromanipulator with millimeter strokes," *IEEE Transactions on Robotics*. doi: 10.1109/TRO.2022.3192778, (in press).

[20] T. C. Duc, G.-K. Lau, and P. M. Sarro, "Polymeric thermal microactuator with embedded silicon skeleton: Part II fabrication, characterization, and application for 2-DOF microgripper," *Journal of Microelectromechanical Systems*, vol. 17, no. 4, pp. 823–831, 2008.

[21] S. Muntwyler, B. E. Kratochvil, F. Beyeler, and B. J. Nelson, "Monolithically integrated two-axis microtensile tester for the mechanical characterization of microscopic samples," *Journal of Microelectromechanical Systems*, vol. 19, no. 5, pp. 1223–1233, 2010.